Journal of the Mechanical Behavior of Biomedical Materials 75 (2017) 521–528

Contents lists available at ScienceDirect

Journal of the Mechanical Behavior of Biomedical Materials

journal homepage: www.elsevier.com/locate/jmbbm

3D-printing zirconia implants; a dream or a reality? An in-vitro study evaluating the dimensional accuracy, surface topography and mechanical properties of printed zirconia implant and discs

Reham B. Osman[a,b], Albert J. van der Veen[c], Dennis Huiberts[b], Daniel Wismeijer[b], Nawal Alharbi[b,d,*]

[a] Department of Removable prosthodontics, Faculty of Dentistry, Cairo University, Egypt
[b] Department of Oral Implantology and Prosthetic Dentistry, Academic Centre for Dentistry Amsterdam (ACTA), University of Amsterdam and Vrije Universiteit Amsterdam, Amsterdam, The Netherlands
[c] Department of Physics and Medical Technology, VU University Medical Centre, Research Institute MOVE, Amsterdam, The Netherlands
[d] Prosthetic Dental Science Department, College of Dentistry, King Saud University, Riyadh, Saudi Arabia

ARTICLE INFO

Keywords:
Custom dental Implant
Zirconia
Additive manufacturing
3D-printing
DLP
CAD/CAM

ABSTRACT

Purpose: The aim of this study was to evaluate the dimensional accuracy, surface topography of a custom designed, 3D-printed zirconia dental implant and the mechanical properties of printed zirconia discs.
Materials and methods: A custom designed implant was 3D-printed in zirconia using digital light processing technique (DLP). The dimensional accuracy was assessed using the digital-subtraction technique. The mechanical properties were evaluated using biaxial flexure strength test. Three different build angles were adopted to print the specimens for the mechanical test; 0°(**V**ertical), 45° (**O**blique) and 90°(Horizontal) angles. The surface topography, crystallographic phase structure and surface roughness were evaluated using scanning electron microscopy analysis (SEM), X-ray diffractometer and confocal microscopy respectively.
Results: The printed implant was dimensionally accurate with a root mean square (RMSE) value of 0.1 mm. The Weibull analysis revealed a statistically significant higher characteristic strength (1006.6 MPa) of 0° printed specimens compared to the other two groups and no significant difference between 45° (892.2 MPa) and 90° (866.7 MPa) build angles. SEM analysis revealed cracks, micro-porosities and interconnected pores ranging in size from 196 nm to 3.3 μm. The mean Ra (arithmetic mean roughness) value of 1.59 μm (± 0.41) and Rq (root mean squared roughness) value of 1.94 μm (± 0.47) was found. A crystallographic phase of primarily tetragonal zirconia typical of sintered Yttria tetragonal stabilized zirconia (Y-TZP) was detected.
Conclusions: DLP prove to be efficient for printing customized zirconia dental implants with sufficient dimensional accuracy. The mechanical properties showed flexure strength close to those of conventionally produced ceramics. Optimization of the 3D-printing process parameters is still needed to improve the microstructure of the printed objects.

1. Introduction

Since their introduction, dental implants have proven successful for rehabilitation of partially and completely edentulous patients. Commercially available implants provide limited design options in terms of implant length, diameter and emergence profile. Given the wide variety of individual oral conditions and clinical situations, customized dental implants can fill the gap between the available standard designs and the patient's oral conditions. Furthermore, rehabilitation time could be reduced, presenting a promising prospective for implant dentistry (Chen et al., 2014).

Rapid developments in the field of biomaterials and computer-aided design/computer-aided manufacturing (CAD/CAM) technology revived interest in customized implants. Additive manufacturing (AM), also known as 3D printing, allows for customization, producing nearly any geometry without the use of expensive molds and tooling required for conventional milling technique (Chen et al., 2014).

Of equally growing popularity, are zirconia implants made from yttria-stabilized tetragonal zirconia polycrystals (Y-TZP) (Osman and Swain, 2015). Available data from *in- vitro* and *in- vivo* clinical studies

* Correspondence to: Department of Oral Implantology and Prosthetic Dentistry, Academic Centre for Dentistry Amsterdam (ACTA), Gustav Mahlerlaan 3004, 1081 LA Amsterdam, The Netherlands.
E-mail address: nawalmurshed@gmail.com (N. Alharbi).

http://dx.doi.org/10.1016/j.jmbbm.2017.08.018
Received 16 June 2017; Received in revised form 12 August 2017; Accepted 14 August 2017
Available online 16 August 2017

reveal favorable biocompatibility and osseointegration compared to standard titanium implants (Depprich et al., 2008; Dubruille et al., 1999; Gahlert et al., 2012; Hoffmann et al., 2008; Scarano et al., 2003; Schultze-Mosgau et al., 2000). Yttria-stabilized tetragonal zirconia polycrystals (Y-TZP), exhibits improved mechanical properties, superior corrosion and wear resistance that makes it a suitable substrate for fabricating dental implants Denry and Kelly (2008); Piconi and Maccauro, 1999). Furthermore, zirconia implants satisfy the increasing aesthetic demands and metal-free requests of a large proportion of dental patients.

AM methods using zirconia can largely be divided into two groups: stereolithography/digital light processing (SLA/DLP) (Lee and Jiang, 2014; Mitteramskogler et al., 2014) and direct deposition printing/jetting (Ebert et al., 2009; Silva et al., 2011). SLA/DLP use a photochemical reaction wherein a photosensitive liquid polymer is cured as the model is built layer by layer (Al Mortadi et al., 2012; Melchels et al., 2010). However, challenges inherent to layer manufacturing must not be underestimated. These include but are not limited to surface quality, dimensional accuracy and the mechanical properties of the final printed object (Oropallo and Piegl, 2016).

Comprehensive studies evaluating the various aspects of DLP-processed custom designed zirconia dental implants have yet to be reported. Hence, the purpose of this study was to evaluate the dimensional accuracy and surface topography of a customized zirconia dental implant printed using DLP technology. Further, to evaluate the flexure strength of the printed material. The mechanical properties and surface topography of printed zirconia implant and discs were evaluated using *in-vitro* experimental studies whereas the dimensional accuracy was assessed using a digital subtraction technique.

2. Materials and methods

2.1. Printing of the implant

A custom one-piece dental implant was designed and 3D-printed in TZ-3YS-E using a DLP-technique. Fig. 1 shows the digital file of the designed custom implant and the 3D-printed implant. TZ-3YS-E was mixed with photocurable resin to form ceramic slurry; the detailed material composition is shown in Table 1. The digital data of the designed implant was exported in Standard Tessellation Language format (STL). The implant was printed using a DLP printer (ADMAFLEX 2.0; ADMATEC Europe BV, The Netherlands) at the center of the build platform and at 0 ° angle (vertically with no tilting of the implant) and the support structure were attached to the apical portion of the implant. The DLP printer involves an LED light source, DMD device/chip, lens, resin vat, and a build platform that is moving in Z-axis. The size of build platform was 53.58 × 95.25 mm and the power of resolution was 1080 ×1920 pixels. The pixel size was 49.61 μm and the layer thickness was 30 μm. After printing, the green body was exposed to a debinding process to burn out all the organic binder components. Afterwards the porous brown body underwent a sintering process with a maximum temperature of 1500 °C to obtain fully densified specimens (99.8% average, 99.9%, maximum 99.7% minimum) as per the manufacturer. An illustration of the 3D-printing process is presented in Fig. 2.

Table 1
Material Composition as per manufacturer.

Powder composition	
Y_2O_3 (mol%)	3
Actual Partical Size (μm)	0.09 (90 nm)
Y_2O_3 (wt%)	5.2 ± 0.5
HfO_2 (wt%)	< 5
Al_2O_3 (wt%)	≤ 0.1–0.4
SiO_2 (wt%)	≤ 0.02
Fe_2O_3 (wt%)	≤ 0.01
Na_2O (wt%)	≤ 0.06
Pigment (wt%)	–
Specific Surface Area (m^2/g)	7 ± 2

2.2. Digital subtraction technique

The dimensional accuracy was evaluated using digital subtraction technique (Alharbi et al., 2016b). The printed implant was scanned using a high-resolution optical surface scanner (IScan D104i; Imetric 3D SA; Courgenay, Switzerland). The file of the scanned printed implant (test model) was saved in STL format. STL file of the test model was exported and superimposed with the STL file of the designed implant (reference model) using Geomagic® studio; 2014 (3D Systems, Rock Hill, SC, USA) (Alharbi et al., 2016b).

The average deviation and the root mean square estimate (RMSE) between the STL files of the reference and test models were calculated. Furthermore, the resultant color map was assessed. One trained operator performed the scanning procedure and the measurements for the specimens.

2.3. Biaxial flexure strength test

To determine the strength of the DLP-printed zirconia material, biaxial flexure test following the ISO 6872:2008 standard, characteristic strength and Weibull moduli analysis were performed.

Forty-five disc-shaped specimens were DLP- printed in yttria-stabilized zirconia dental material (TZ-3YS-E), same material that was used

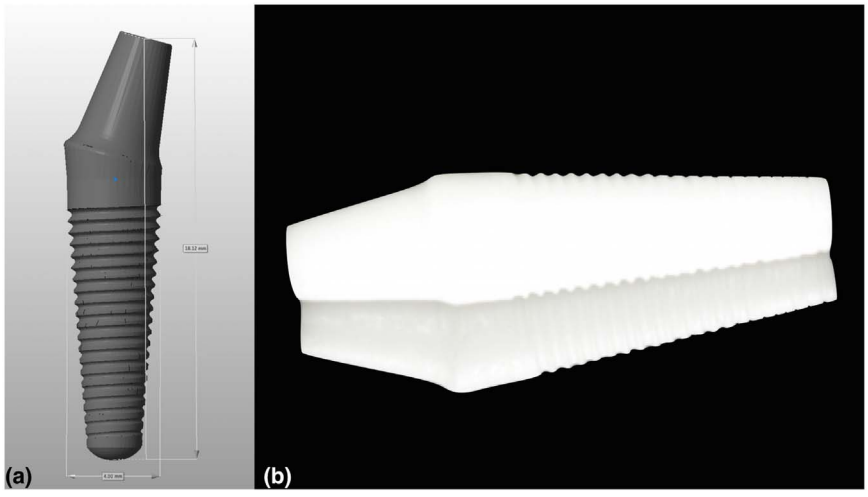

Fig. 1. (a) 3D-CAD design of implant, (b) Printed zirconia implant.

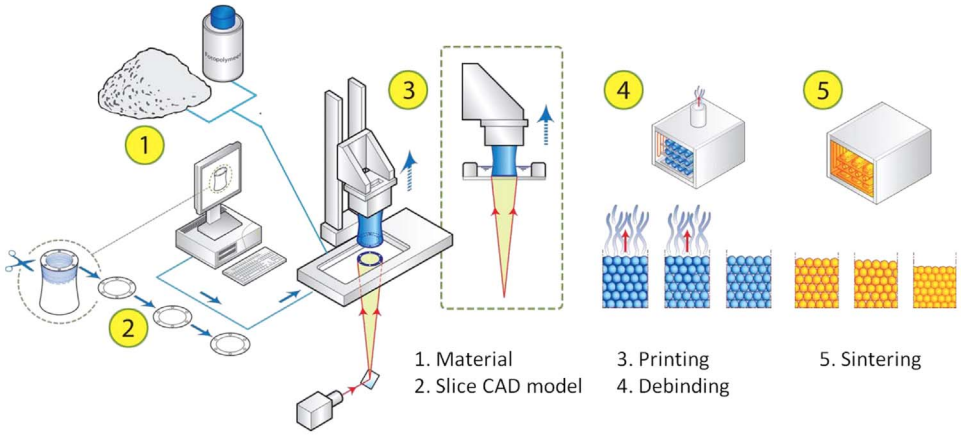

Fig. 2. Illustration of the 3D-printing fabrication process. Adopted from ADMATEC Europe BV.

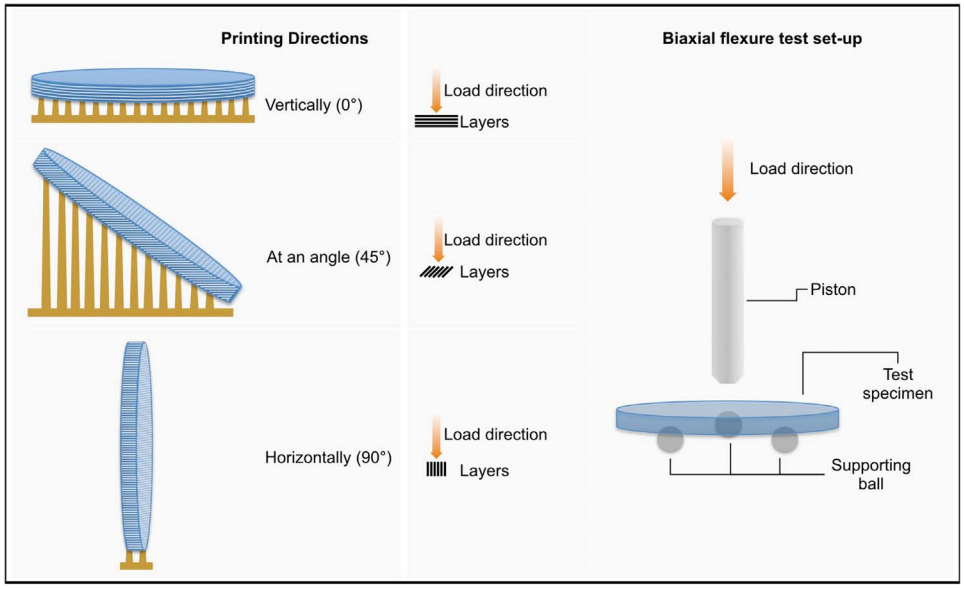

Fig. 3. Specimen orientations during build process and mechanical test set-up.

for the printing of the designed implant. All specimens were disc-shape with an average diameter of 15 ± 0.12 mm and an average thickness of 1.2 ± 0.02 mm. The specimens were divided into three groups; 15 discs per group based on the build direction (layer orientation). In the first group the discs were printed vertically (V) at 0°; the layers were stacked on top of each other along the height of the specimen and were perpendicular to load direction. In the second group the specimens were obliquely tilted (O) so that the layers were at 45° to the load direction. In the third group the specimens were printed at 90° (H); the layers were staked alongside each other through the length of the specimen and the layers were parallel to load direction (Fig. 3).

Bi-axial flexure test was performed using universal testing machine (Instron 8872; Instron) applying an increasing load of 10 kN at cross-head speed of 1 mm/min until catastrophic failure of discs. Prior to the test, the discs were visually inspected for any defects, support structures were removed and the surface was finished and polished by the manufacturer. The maximum load required to fracture the specimen was recorded.

2.4. SEM and surface roughness

To analyze the surface topography of the printed material, SEM micrographs at different magnifications (ZEISS MERLIN HR; Germany) were made for printed implant, representative specimens from the printed material and from the fractured discs following the biaxial flexure test. The specimens were sputter coated with gold at a thickness of 10–15 nm. Surface roughness of printed implant was measured quantitatively by arithmetic mean value of the profile (Ra), root mean square average of the profile RMS (Rq) using confocal microscopy (Leica SP2 Microsystems, Heidelberg GmbH) (Park et al., 2015). An evaluation length of 0.09 mm profile was defined, randomly distributed over the screw part of the implant (n = 10). The roughness measurements were calculated using Leica confocal processing software Leica Microsystems, Heidelberg GmbH version 2.61 Build 1537.

2.5. X-ray diffractometer

Crystallographic phase analysis of the printed material was performed using an x-ray diffractometer (Bruker AXS, D8 Advance, Karlsruhe, Germany). Test was performed at 2θ range of 25–35° and at a step interval of 1 s and step size of 0.03°.

2.6. Statistical analysis

The results were statistically analyzed using SPSS statistics for MAC. The data were checked for normality distribution and equivalence of variance. Descriptive statistics were calculated and analysis of the variance (ANOVA) test was used to detect difference in flexure strength between the groups. Statistical significance was set at $P = 0.05$. Least significant difference (LSD) post hoc test was also performed to further

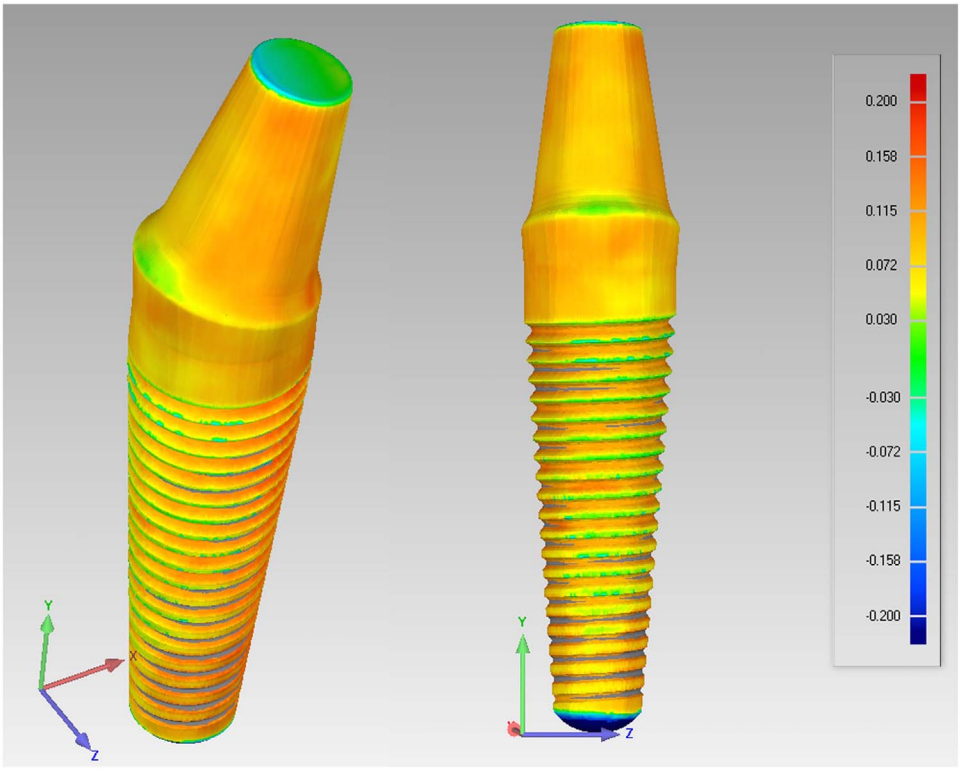

Fig. 4. Color map of the scanned printed zirconia implant showing 3D- deviation pattern.

analyze the difference between the groups. Further, Weibull modulus (m) and the characteristic strength (σ_c) were calculated with a confidence interval of 95%, according to DIN EN 843-5 test (Pereira et al., 2016).

3. Results

3.1. Dimensional accuracy of printed implant

The implant was successfully 3D-printed as shown in Fig. 1b. The root mean square estimate was 0.1 mm. The average deviation was 0.089 and −0.129 mm (± 0.068) homogenously distributed along the length of the printed implant as evident by the assessment of the color map (Fig. 4). Different colors represent the distance between the corresponding points on the reference and test models and are indicated by the scale bar (Fig. 4). Dark red and blue colors at top and bottom of bar indicates +0.200 mm and −0.200 mm deviations respectively. Blue color (negative deviation) observed at the apex of the implant is due to support removal.

3.2. Mechanical properties of printed material

The mean and standard deviation of the flexure strength, characteristic strength and Weibull moduli values for all groups are presented in Table 2. One specimen from 45° group was lost during the test. The result of the ANOVA was ($F = 3.4$; $df = 43$; $P = 0.04$).

Least significant difference (LSD) post hoc test showed that specimens printed vertically at 0°(V) exhibit a statistically significant higher strength value (943.2 MPa) than specimens printed obliquely at 45° (O) (822.3 ± 172 MPa) ($P = 0.024$) and than those printed horizontally at 90°(H) (834.4 ± 72 MPa) ($P = 0.03$). There was no difference between specimens printed at 45° (O) and at 90° (H) angles ($P = 0.8$).

The Weibull analysis revealed a statistically significant difference in characteristic strength (1006.6 MPa) of 0°(V) printed specimens compared to the other two groups and no difference between 45°(O) (892.2 MPa) and 90°(H) (866.7 MPa) printed groups (Table 2).

Table 2
Flexure strength, characteristic strength and Weibull modulus.

Test group	N	Mean σ (SD)	σ_c (CI 95%)	m (CI 95%)
V (0°)	15	943.26 (152.75)	1006.654 (917.66 – 1104.62)	7.032 (4.06–9.82)
O (45°)	14	822.35 (172.71)	892.260 (784.02 – 1015.83)	5.266 (2.96–7.42)
H (90°)	15	834.47 (72.81)	866.722 (824.65 – 910.79)	13.125 (7.58–18.33)

σ: Flexure strength σ_c: Characteristic strength; m: Weibull modulus.

The recorded Weibull modulus (reliability) ranged from 5.3 to 13 with no significant difference between the vertically and horizontally printed groups. Specimens printed at 45° (O) group showed the highest data variability (m value = 5.2), thus more specimens are expected to fail at lower strength (Table 2). The survival probability distribution plot is shown in Fig. 5, the slope as well as the variation of the data indicates the difference in Weibull moduli and characteristic strength between the groups.

3.3. Surface topography of printed implant

The SEM analysis of representative specimen, cross-section of the fractured specimens and printed implants revealed several microcracks, porosities and interconnected pores as shown in Figs. 6–8. The micro-porosities of the representative intact specimens ranged in size from 196 nm to 3.3 μm (Fig. 7c). Quantitative measurement of surface roughness showed a mean Ra value of 1.59 μm (± 0.41) and Rq value of 1.94 μm (± 0.47) (Fig. 9).

3.4. Phase analysis

As expected, the three specimens' representative of the three tested groups showed the standard pattern for sintered Y-TZP; primarily

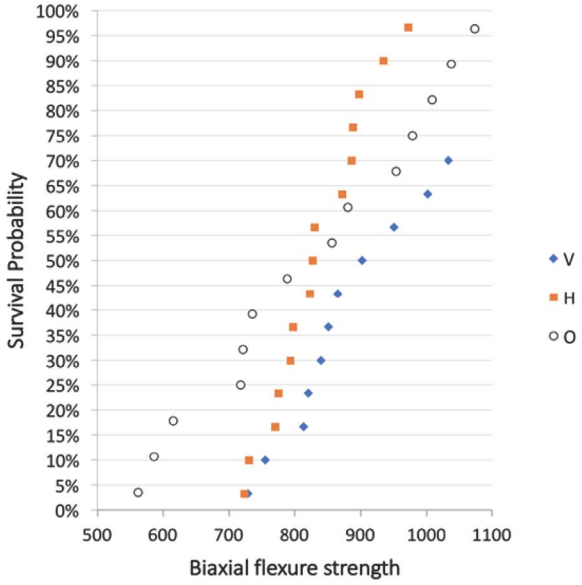

Fig. 5. Survival probability plot.

tetragonal zirconia with very little difference between the three groups (Fig. 10).

4. Discussion

The aim of the study was to evaluate the possibility of printing a custom designed zirconia implant using DLP technology. The dimensional accuracy, surface topography of a printed zirconia implant and mechanical properties of printed zirconia discs were also evaluated.

The dimensional accuracy was evaluated using both RMSE value and the assessment of the color map. Furthermore, the flexure strength was evaluated for the build angles that offer the highest dimensional accuracy, least printing time and least surface roughness (Lee and Jiang, 2014; Osman et al., 2017). In this study, the definition of build direction was based on how the layers were staked along the long axis of the specimen. Vertically, the layers were staked along the height of the specimen, whereas for the horizontally printed group the specimens were tilted 90° from vertical position. The mechanical flexure test was performed on disc-shaped specimens that may not represent the actual clinical situation. However, it was performed at this early stage to have a basic understanding of the mechanical properties of the printed material. Further, simpler structures are more amenable to simple analysis and better interpretation (Alharbi et al., 2016a).

DLP may prove to be an efficient mean for printing customized dental implants with sufficient dimensional accuracy. The dimensional accuracy of the printed implant was high and close to the reference model dimensions. The mechanical test suggested that DLP-printed zirconia material exhibited high flexure strength value (943 MPa) comparable to that of milled zirconia (800–1000 MPa) (Denry and Kelly, 2008b). The DLP-printed ceramic object should be favorably manufactured in a vertical direction at 0-degree angle on the build platform, where the layers are perpendicular to the force direction. The 0-degree, vertical build orientation resulted in the highest flexure strength values, whereas the lowest values were observed with 45 degrees build angle. This may be attributed to the difficulty in attachment of subsequent layers of the disc shape experienced with 45° build angle resulting in more structural defects of printed object.

The Weibull modulus (m) describes the distribution of the strength, thus the lower the value, the more the reliability of the results. The recorded Weibull modulus ranged from 5.3 to 13, which falls within the range reported for current Y-TZP 4.31–21.59) (Karakoca and Yılmaz, 2009; Pereira et al., 2015, 2014). The increased variability (range) of Weibull modulus values for specimens printed at 45° may be attributed to the vector of the applied force. The vertically 0-degree printed specimens had layers that are perpendicular to the applied force and in a different direction than the detected inter-layer cracks and porosities. Another possible explanation, previously mentioned, is the difficulty in attachment of subsequent layers experienced during the 45°-build process resulting in more structural defects of printed object. The failure analysis revealed that approximately 63.2% or less of the specimens printed at 0° (V), and 82.6% of the specimens printed at 45° group (O) and 100% of the specimens printed at 90° (H) will have failed at or below 1006.6 MPa. All values are equal/beyond the flexure strength value reported for conventionally used zirconia used as an implant substrate (900–1200 MPa) (Hisbergues et al., 2009; Osman et al., 2013). The observed surface roughness (Ra 1.59 μm) of the printed zirconia implant fall well within the range of moderately rough surface (1.0–2.0 μm) reported for titanium implant by Albrektsson & Wennerberg to have optimal bone response needed for osseointegration (Albrektsson and Wennerberg, 2004).

Yet, similar to other AM methods, DLP manufacturing technique still presents challenges inherent to layering technique and sintering processes of the printed parts (Lee and Jiang, 2014; Oropallo and Piegl, 2016). Post-processing of ceramic green parts involves thermal sintering. Micro-cracks evident on the surface of printed implant and representative specimens may be attributed to the shrinkage of the built up layered structure during the sintering process. It suggests the bonding between the layers is less than within the printed layer and affects the mechanical strength of the sintered part (Zocca et al., 2015). Either two-stage sintering or slow temperature ramps are suggested to prevent sudden temperature fluctuations and thus the occurrence of micro-cracks. Altering the grain size can further influence the microstructure and mechanical properties of the sintered part. The latter can be achieved by manipulating the temperature during sintering process (Yu et al., 2007).

The SEM micrograph of the representative fractured specimens revealed porosities ranging in size from 196 nm to 3.3 μm, some of which

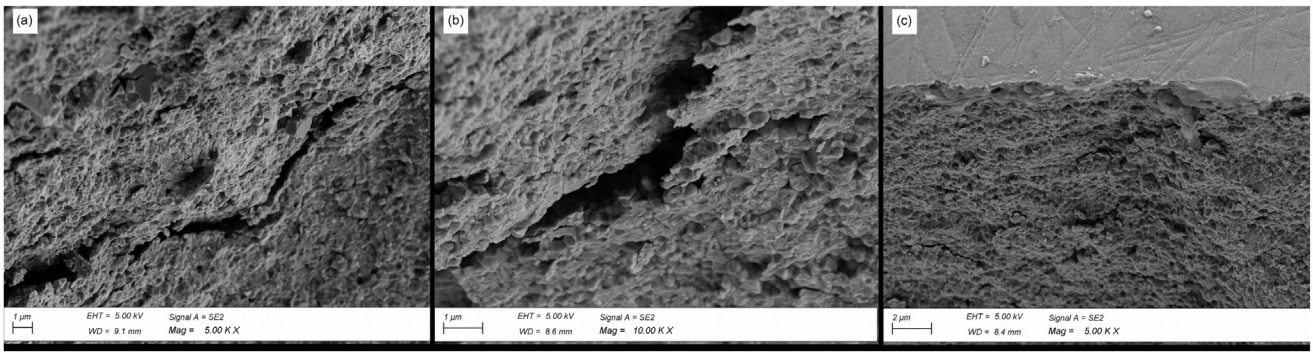

Fig. 6. SEM of fractured specimens for 3 build angles: (a) 0°, (b) 45°, (c) 90°.

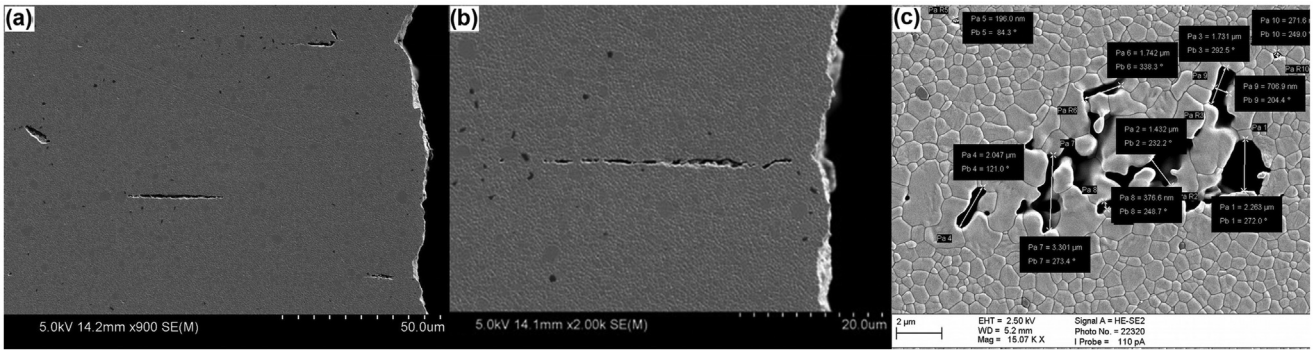

Fig. 7. Cracks, porosities and interconnected pores in the representative printed specimens, (a) Mag 900×, (b) Mag 2000×, (c) Mag 15000×.

were deeply connected within the structure of the material. The precise cause of the observed flaws would require further detailed investigation. The possible evaporation of the solvent in the polymer loaded printed ceramic slurry on the exposed surface during the printing and before the next layer is printed may lead to differential shrinkage upon sintering and as such the cracking and porosities observed. In the same context, insufficient amount of ceramic particles in the dispersion or the type of the resin used may also be contributing factors. Future research should therefore focus on printable powder composition, while keeping the rheological behavior unchanged (Faes et al., 2015). This for example can be achieved through the introduction of steric repulsive forces in the dispersion. The curing light source should also be investigated to be adequate for the intended purpose. Low irradiance and a non-optimal match with the polymerization wavelength of the used resin may result into partial polymerization of the printed layers. This will necessitate the need for an extra, thermal polymerization step. Such a step may result in a bimodal grain size distribution, which may well be increasing the susceptibility of the zirconia to low temp degradation (LTD) specifically when tested in intra-oral clinical situation. In order to eliminate this extra, time-consuming step and all related consequences, a better matched light-source that is compatible with printable powder composition is thus desirable. During the debinding process, the binder burnout of voluminous compact structures may be extremely difficult and even worse would lower the packing density of processed part resulting in enhanced sintering shrinkage, and a challenging situation to obtain net shape parts after sintering (Zocca et al., 2015).

From the findings of this study, it can be concluded that the microstructure of the DLP-processed implants combined with post surface treatment should be studied intensively to achieve better structure of the printed material. Future trials should focus on the 3D-printing of ceramic parts that are free of cracks and porosities similar to the microstructure of conventionally milled ceramics. Manufacture of such parts can be achieved via optimizing the parameters of AM process or performing extra densification steps following the completion of printing process (Deckers et al., 2014). Further *in- vitro* and *in- vivo* animal studies for the evaluation of DLP-processed one-piece zirconia implants are still mandatory before pursing the advanced technology for customizing, designing, and printing zirconia implants and delivering the treatment to patients using full digital workflow.

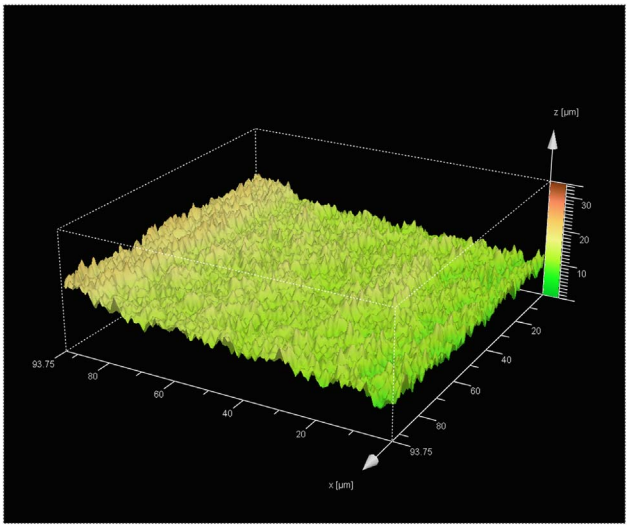

Fig. 9. 3D-topographical image of the printed zirconia implant (93 × 93) µm.

Conflict of interest

The authors have no conflict of interest related to the content of the submission.

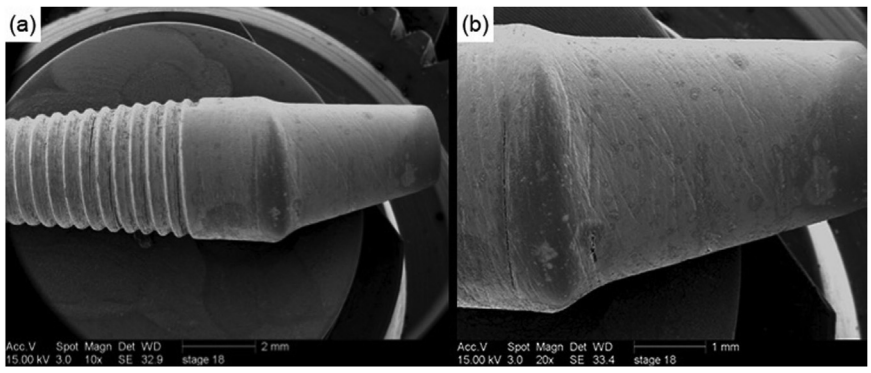

Fig. 8. SEM of the printed implant. (a) Mag 10×, (b) Mag 20×.

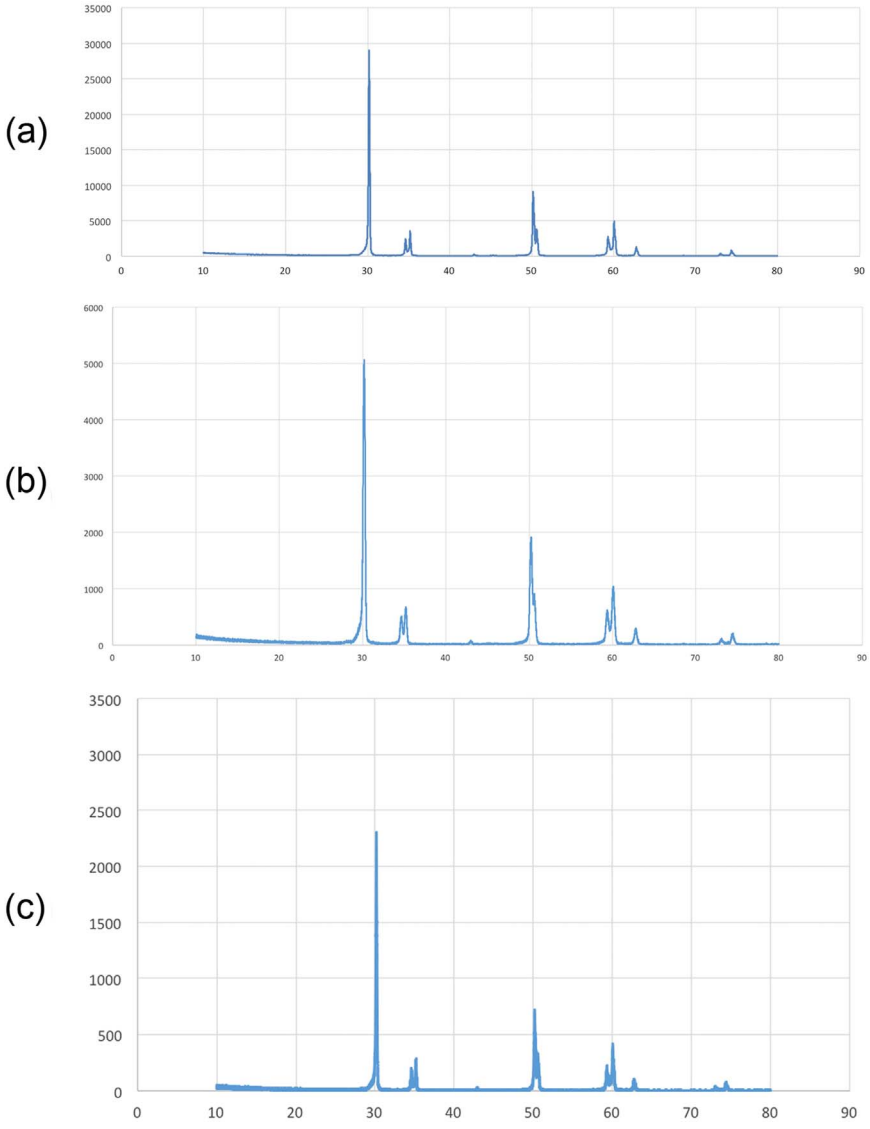

Fig. 10. XRD spectra of the three build angles; (a) build angle 0°, (b) build angle 45°, (c) build angle 90°.

Acknowledgment

The authors would like to thank Dr. Wael Aboelso'oud for his contribution in designing the implant and Cor Semeins for his technical assistance during confocal microscopy. This project is supported by a scholarship (grant number 25/302626) from King Saud University, Riyadh, Kingdom of Saudi Arabia.

References

Al Mortadi, N., Eggbeer, D., Lewis, J., Williams, R.J., 2012. CAD/CAM/AM applications in the manufacture of dental appliances. Am. J. Orthod. Dentofac. 142, 727–733.

Albrektsson, T., Wennerberg, A., 2004. Oral implant surfaces: Part 1–review focusing on topographic and chemical properties of different surfaces and in vivo responses to them. Int. J. Prosthodont 17, 536–543.

Alharbi, N., Osman, R., Wismeijer, D., 2016a. Effects of build direction on the mechanical properties of 3D-printed complete coverage interim dental restorations. J. Prosthet. Dent. 115, 760–767.

Alharbi, N., Osman, R., Wismeijer, D., 2016b. Factors influencing the dimensional accuracy of 3D-printed full coverage dental restorations using stereolithography technology. Int. J. Prosthodont 29, 503–510.

Chen, J., Zhang, Z., Chen, X., Zhang, C., Zhang, G., Xu, Z., 2014. Design and manufacture of customized dental implants by using reverse engineering and selective laser melting technology. J. Prosthet. Dent. 112, 1088–1095.

Deckers, J., Vleugels, J., Kruth, J.-P., 2014. Additive manufacturing of ceramics: a review. J. Ceram. Sci. Technol. 5, 245–260.

Denry, I., Kelly, J.R., 2008. State of the art of zirconia for dental applications. Dent. Mater. 24, 299–307.

Depprich, R., Zipprich, H., Ommerborn, M., Mahn, E., Lammers, L., Handschel, J., Naujoks, C., Wiesmann, H.-P., Kübler, N.R., Meyer, U., 2008. Osseointegration of zirconia implants: an SEM observation of the bone-implant interface. Head Face Med. 4, 1.

Dubruille, J.-H., Viguier, E., Le Naour, G., Dubruille, M.-T., Auriol, M., Le Charpentier, Y., 1999. Evaluation of combinations of titanium, zirconia, and alumina implants with 2 bone fillers in the dog. Int. J. Oral. Maxillofac. Implants 14, 271–277.

Ebert, J., Ozkol, E., Zeichner, A., Uibel, K., Weiss, O., Koops, U., Telle, R., Fischer, H., 2009. Direct inkjet printing of dental prostheses made of zirconia. J. Dent. Res. 88, 673–676.

Faes, M., Valkenaers, H., Vogeler, F., Vleugels, J., Ferraris, E., 2015. Extrusion-based 3D printing of ceramic components. Procedia CIRP 28, 76–81.

Gahlert, M., Roehling, S., Sprecher, C.M., Kniha, H., Milz, S., Bormann, K., 2012. In vivo performance of zirconia and titanium implants: a histomorphometric study in mini pig maxillae. Clin. Oral. Implants Res. 23, 281–286.

Hisbergues, M., Vendeville, S., Vendeville, P., 2009. Zirconia: established facts and perspectives for a biomaterial in dental implantology. J. Biomed. Mater. Res. Part B: Appl. Biomater. 88, 519–529.

Hoffmann, O., Angelov, N., Gallez, F., Jung, R.E., Weber, F.E., 2008. The zirconia implant-bone interface: a preliminary histologic evaluation in rabbits. Int. J. Oral. Maxillofac. Implants 23, 691.

Karakoca, S., Yılmaz, H., 2009. Influence of surface treatments on surface roughness, phase transformation, and biaxial flexural strength of Y-TZP ceramics. J. Biomed. Mater. Res. Part B: Appl. Biomater. 91, 930–937.

Lee, S.-Y., Jiang, C.-P., 2014. Development of a three-dimensional slurry printing system using Dynamic mask projection for Fabricating zirconia dental implants. Mater. Manuf. Process. 30, 1498–1504.

Melchels, F.P., Feijen, J., Grijpma, D.W., 2010. A review on stereolithography and its applications in biomedical engineering. Biomaterials 31, 6121–6130.

Mitteramskogler, G., Gmeiner, R., Felzmann, R., Gruber, S., Hofstetter, C., Stampfl, J., Ebert, J., Wachter, W., Laubersheimer, J., 2014. Light curing strategies for

lithography-based additive manufacturing of customized ceramics. Addit. Manuf. 1–4, 110–118.
Oropallo, W., Piegl, L.A., 2016. Ten challenges in 3D printing. Eng. Comput. 32, 135–148.
Osman, R., Alharbi, N., Wismeijer, D., 2017. Build angle, does it have an influence on the accuracy of 3D-printed dental restorations using digital light-processing technology? Int. J. Prosthodont 30, 182–188.
Osman, R.B., Elkhadem, A.H., Ma, S., Swain, M.V., 2013. Titanium versus zirconia implants supporting maxillary overdentures: three-dimensional finite element analysis. Int. J. Oral. Maxillofac. Implants 28, 198–208.
Osman, R.B., Swain, M.V., 2015. A critical review of dental implant materials with an emphasis on titanium versus zirconia. Materials 8, 932–958.
Park, J.B., Jeon, Y., Ko, Y., 2015. Effects of titanium brush on machined and sand-blasted/acid-etched titanium disc using confocal microscopy and contact profilometry. Clin. Oral. Implants Res. 26, 130–136.
Pereira, G.K.R., Amaral, M., Cesar, P.F., Bottino, M.C., Kleverlaan, C.J., Valandro, L.F., 2015. Effect of low-temperature aging on the mechanical behavior of ground Y-TZP. J. Mech. Behav. Biomed. Mater. 45, 183–192.
Pereira, G.K.R., Amaral, M., Simoneti, R., Rocha, G.C., Cesar, P.F., Valandro, L.F., 2014. Effect of grinding with diamond-disc and-bur on the mechanical behavior of a Y-TZP ceramic. J. Mech. Behav. Biomed. Mater. 37, 133–140.
Pereira, G.K.R., Silvestri, T., Camargo, R., Rippe, M.P., Amaral, M., Kleverlaan, C.J., Valandro, L.F., 2016. Mechanical behavior of a Y-TZP ceramic for monolithic restorations: effect of grinding and low-temperature aging. Mater. Sci. Eng. C Mater. Biol. Appl. 63, 70–77.
Piconi, C., Maccauro, G., 1999. Zirconia as a ceramic biomaterial. Biomaterials 20, 1–25.
Scarano, A., Di Carlo, F., Quaranta, M., Piattelli, A., 2003. Bone response to zirconia ceramic implants: an experimental study in rabbits. J. Oral. Implantol. 29, 8–12.
Schultze-Mosgau, S., Schliephake, H., Radespiel-Tröger, M., Neukam, F.W., 2000. Osseointegration of endodontic endosseous cones Zirconium oxide vs titanium. Oral. Surg. Oral. Med. Oral. Pathol. Oral. Radiol. Endod. 89, 91–98.
Silva, N.R., Witek, L., Coelho, P.G., Thompson, V.P., Rekow, E.D., Smay, J., 2011. Additive CAD/CAM process for dental prostheses. J. Prosthodont 20, 93–96.
Yu, P.C., Li, Q.F., Fuh, J.Y.H., Li, T., Lu, L., 2007. Two-stage sintering of nano-sized yttria stabilized zirconia process by powder injection moulding. J. Mater. Process Technol. 192, 312–318.
Zocca, A., Colombo, P., Gomes, C.M., Günster, J., 2015. Additive manufacturing of ceramics: issues, potentialities, and opportunities. J. Am. Ceram. Soc. 98, 1983–2001.